Journal of the Physical Society of Japan
Vol. 52, No. 1, January, 1983, pp. 94–99

Effect of Decay Index on Elongation Ratio in Non-Circular Tokamak TNT-A

Shunjiro SHINOHARA, Kaichiro SAKUMA
Yoshio NAGAYAMA and Hiroshi TOYAMA

Department of Physics, Faculty of Science,
University of Tokoy, Bunkyo-ku, Tokyo 113

(Received December 17, 1981)

In a non-circular tokamak (TNT-A), the relation between elongation ratio κ and decay index n ($=-(r/B_z)\cdot(\partial B_z/\partial r)$) is investigated, varying the curvature of the shaping field. Both active and passive control have been done in the region of $-0.9<n<-0.2$. By Thomson scattering, magnetic probes and flux loops measurements, a D-shaped, stable plasma of $T_{e0}\sim 180$ eV, $n_{e0}\sim 10^{13}$ cm^{-3}, $q_a>2$ (the MHD oscillation of $m=2$ mode appears) with elongation ratio of up to 1.5 is obtained. The numerical curve of plasma equilibrium in (κ, n) space fits well with the measurements. The effects of the iron core and shell on the decay index are important in a non-circular tokamak. The iron core makes the decay index lower, and the shell makes the field curvature smaller. The calculation and measurements show that the decay index is mainly affected by the iron core.

§1. Introduction

It is generally considered that a non-circular plasma cross section[1-3] will be a necessary feature of a tokamak fusion reactor. The results from Doublet IIA[4] show enhancement of the $n_e\tau_e$ product (n_e: electron density, τ_e: energy confinement time) with elongation ratio κ ($=b/a$: ratio of height to horizontal semi axis length). The measurements in TOSCA[5-7] show that τ_e and poloidal beta value increase with elongation ratio, and a central beta value of 4% was obtained for a triangular plasma. In Doublet III,[8,9] the maximum plasma current increases almost linearly with elongation ratio, and the high current operation capability of D-shaped plasmas produces a remarkable improvement in energy confinement time ($\propto 1+\kappa^2$).

In the INTOR[10] design, the plasma has elongation ratio of 1.6 with D-shape. The feasibility of shaping plasmas into vertically elongated configurations, and the effect of this shaping on plasma stability and confinement are important for reactor design.

In order to produce the desired shape of the plasma, we must know the dependence of the plasma shape on the shaping field curvature. In this paper, the effect of the decay index, $n=-r/B_z\cdot\partial B_z/\partial r$, on elongation ratio is investigated in a non-circular tokamak TNT-A.[11-13] We measure the electron temperature profile and magnetic surface of the vertically elongated plasma (§3). In §4, we compare the measured value of the decay index with the calculated one, considering the effect of the iron core and shell. After determining the decay index, we present the dependence of elongation ratio, the maximum plasma current, mean current density and safety factor on the decay index in §5. Finally, the conclusion is presented in §6.

§2. Device

TNT-A is a non-circular tokamak with major radius $R_0=40$ cm and toroidal field $B_t\leq 4.4$ kG. Its schematic view is illustrated in Fig. 1. The vacuum chamber has a rectangular cross section of 24 cm wide and 60 cm high. The plasma volume is limited by a molybdenum limiter with a D-shaped aperture of 18 cm wide and 36 cm high. The plasma current is driven by an iron core transformer with a flux of 0.15 V·sec. The plasma shape is controlled by the external shaping field generated by eight shaping coils (10 turns each) around the chamber. In addition, a copper shell (10 mm thick), on inside

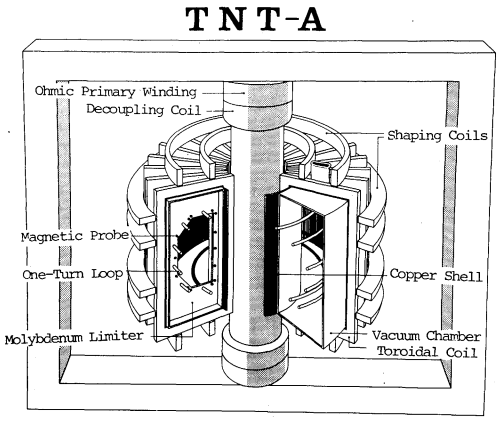

Fig. 1. Schematic view of TNT-A.

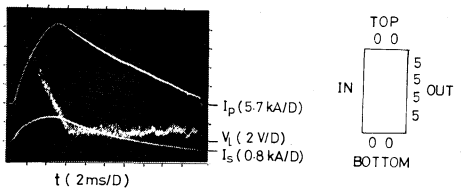

Fig. 2. Typical example of discharge under active control together with number of turns of shaping coils. Plasma current I_p (5.7 kA/D), loop voltage V_l (2V/D) and shaping current I_s (0.8 kA/D) are shown.

only, restricts the magnetic surface.

§3. Non-Circular Plasma

Experiments were done to establish the relation between the plasma shape and decay index at $B_t=4.2$ kG. The optimization was carried out to obtain the larger plasma current, lower loop voltage and longer discharge duration, and to locate the plasma column near the center of the limiter.

Figure 2 shows a typical discharge under the active control with of five turns each four outer shaping coils. In this case, $\bar{n}_v=-0.25$. ($\bar{n}_v$ is the averaged decay index calculated over the plasma cross section, neglecting the effects of the iron core and shell.) Figure 3 shows the contour map of the electron temperature, and the magnetic surfaces, including the numerical calculation of plasma equilibrium, at the current peak of $I_p=20$ kA, $V_l=3.5$ V with the same turns of the shaping coils in Fig. 2. The magnetic surface was calculated by the equations $rB_r=-\partial\psi/\partial z$ and $rB_z=\partial\psi/\partial r$ (B_r: poloidal field, ψ: magnetic flux function). In this calculation, 14 magnetic probes and six flux loops around the limiter were used. The distance (Δr, Δz) from the position of a flux loop to that of the one magnetic surface which passes on the other flux loop was estimated by $\Delta z\simeq-\Delta\psi/rB_r$, $\Delta r\simeq\Delta\psi/rB_z$ ($\Delta\psi$: the difference of ψ between the two flux loops). The plasma surface was determined as follows: the top, bottom and outer side of the plasma surface was assumed to be on the place where movable limiters affect the plasma properties (*e.g.*,

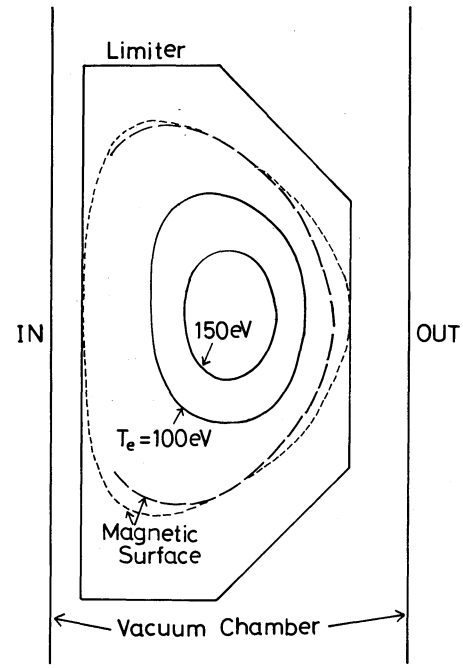

Fig. 3. Contour map of electron temperature in the case of $I_p=20$ kA and $V_l=3.5$ V. Contours were estimated from vertical and radial temperature profiles by Thomson scattering measurements Dashed and dotted lines give magnetic surfaces obtained from magnetic probes and flux loops measurements, and from equilibrium code EQUCIR in the case of $a=9$ cm, $\kappa=1.5$, $\beta_p=0.3$, l_i (internal inductance)$=0.55$, γ (triangularity)$=0.5$ and n_0 (central decay index)$=-0.7$, respectively.

the plasma current decreases by about 5%). The double probes were also used to determine the position of the abrupt change of the saturation current near the plasma surface. The inner side of the plasma surface was assumed to be in contact with the limiter from the measurement of the ratio of the poloidal magnetic fields (B_θ) at the inner and outer equator ($\theta=0°$

and 180°). The plasma surface obtained by this method agrees well with the magnetic surface by flux measurements. The magnetic surface in Fig. 3 shows the plasma is vertically elongated with elongation ratio κ of ~ 1.5. From the Thomson scattering and microwave measurements, the central electron temperature and density were $\sim$ 180 eV, $\sim 10^{13}$ cm^{-3}, respectively. Figure 3 also shows that the contour map of the electron temperature is consistent with the result of the magnetic surface.

§4. Calculation and Measurement of Decay Index

In calculating the decay index, we must take account of the effects of the iron core and shell, which exist in TNT-A. We consider the two ideal cases; there is the iron core only and shell only. From the two cases, the decay index in this device can be estimated. The calculation in each case must be done in the presence of the plasma current as well as the shaping current.

In the cylindrical coordinate, the surface of the iron core or the shell is assumed to exist on the constant radius $r=r_c$ from $z=-\infty$ to ∞. When the shaping current flows at $z=0$ and $r=r_s(r_s>r_c)$, the vector potential is described by

$$A_\phi^{(0)}=\frac{\mu_0 r_s I_s}{2\pi}\int_{-\infty}^{\infty} e^{ikz} K_1(|k|r_s)I_1(|k|r)\,dk, \quad (r<r_s),$$

$$=\frac{\mu_0 r_s I_s}{2\pi}\int_{-\infty}^{\infty} e^{ikz} K_1(|k|r)I_1(|k|r_s)\,dk, \quad (r>r_s). \quad (1)$$

Here, I_s is the shaping current, μ_0 is the permeability in the vacuum and I_n, K_n are modified Bessel functions. The perturbed vector potential $A_\phi^{(1)}$ is derived from $\nabla\times\boldsymbol{A}=\boldsymbol{B}$, $(\nabla\times\boldsymbol{B})_\phi=0$,

$$A_\phi^{(1)}=\frac{\mu_0 r_s I_s}{2\pi}\int_{-\infty}^{\infty} e^{ikz} c(k)K_1(|k|r)\,dk. \quad (2)$$

Here,

$$c(k)=K_1(|k|r_s)\frac{I_0(|k|r_c)}{K_0(|k|r_c)},$$

and

$$c(k)=-K_1(|k|r_s)\frac{I_1(|k|r_c)}{K_1(|k|r_c)},$$

from the boundary condition $B_z=0$ (iron core) and $B_r=0$ (shell) at $r=r_c$, respectively. The pertubed vector potential $A_\phi^{(2)}$ from the plasma current can be calculated according to the current profile and the boundary condition in the same way mentioned above.

Now, we apply eqs. (1) and (2) to TNT-A. Figure 4 shows the flux contours produced by the shaping currents in two cases. The dotted line represents contours in the case of no iron core and no shell, using eq. (1) only. The solid line is calculated in the presence of the iron core ($r_s=15$ cm), using eqs. (1) and (2). From this figure, the iron core makes the decay index lower, especially near the surface of the iron core, i.e., B_z is reduced to about 65% in the center of the vacuum vessel of that in the case of no iron core and no shell. On the other hand, the shell makes the field curvature smaller, especially near the surface of the shell,

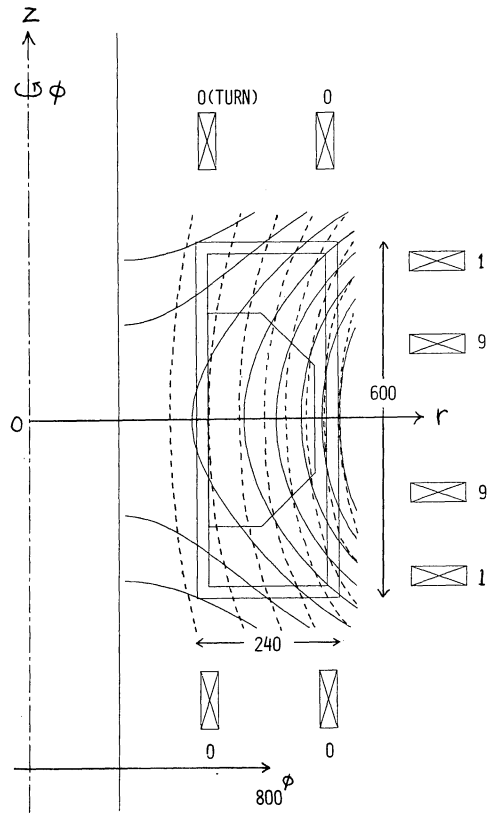

Fig. 4. Flux contours produced by shaping currents. Number of turns of shaping coils is also shown. Dotted line is calculated in the case of no iron core and no shell, and solid line gives contours calculated in the presence of iron core.

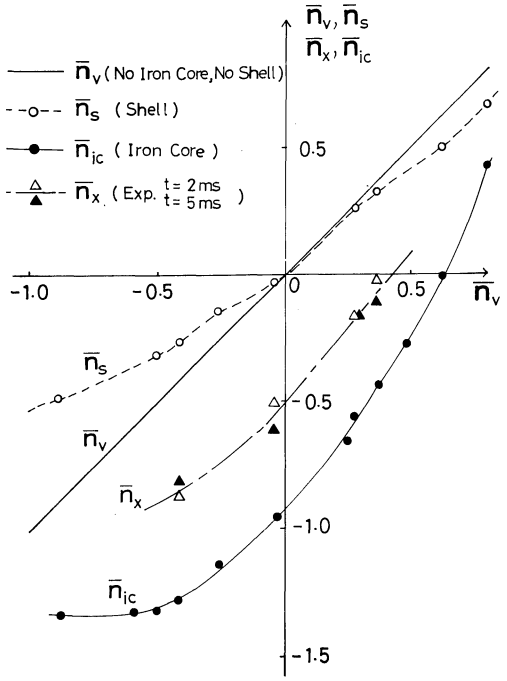

Fig. 5. Relation between various n indices when shaping current flows. Measured value $\bar{n}_x$ is shown at $t=2$ and 5 ms after shaping current flows.

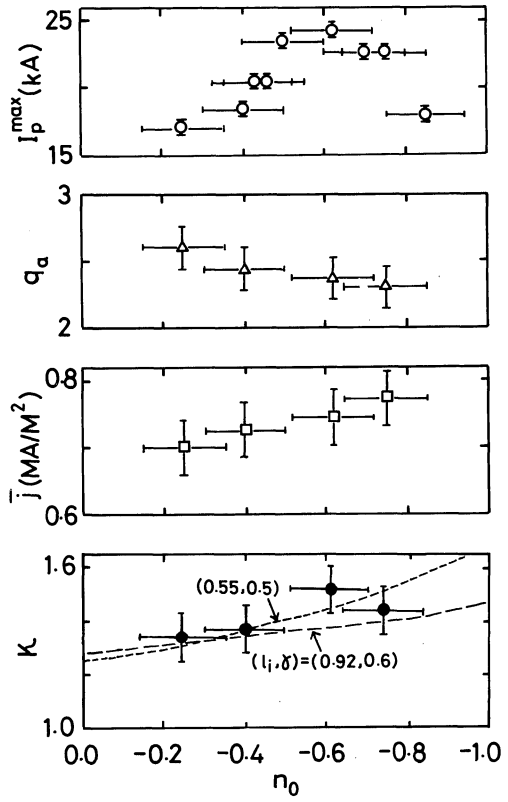

Fig. 6. Dependence of I_p^{max}, q_a, $\bar{j}$ and κ on n_0 under active control. Numerical curves from equilibrium code EQUCIR in the case of $a=9$ cm, $\beta_p=0.3$ is also shown in the lowest graph. Here l_i, γ are internal inductance and triangularity, respectively.

i.e., B_z is larger and B_r is smaller than in the case of no iron and no shell.

Figure 5 shows the relation between the various n indices when the shaping current flows. Here, $\bar{n}_v$ is the mean value calculated in the case of no iron core and no shell. The mean values of n indices, where there exists the iron core and shell, are expressed as $\bar{n}_{ic}$ and $\bar{n}_s$, respectively, while $\bar{n}_x$ is the mean value from the measured vertical field at $z=0$, ± 19.5 cm from $r=31$ to 49 cm. We can see from this figure that the shell makes the field curvaure of the shaping field smaller and the iron core makes the decay index lower. The measured value $\bar{n}_x$ is lower than $\bar{n}_v$ and $\bar{n}_s$ and higher than $\bar{n}_{ic}$. The measured value of B_z is a little larger than the calculated value of B_z in the presence of the iron core. This shows that the shaping field is affected mainly by the iron core. The difference between $\bar{n}_x$ and $\bar{n}_{ic}$ comes from the effects of the shell, the vacuum chamber and the supports of the chamber.

§5. Dependence of Decay Index

In §4, we compared the measured value of the decay index n_x with the calculated one. In the presence of the plasma current, the real decay index n is different from n_x by the effect of the iron core and shell. We derive n from the magnetic and flux loops measurements, using a least squares method to fit the data points to a finite current filament model.[14] The value of n at the plasma center ($n=n_0$) is a little higher than that of n_x by ~ 0.1.

Figure 6 is the dependence of the maximum plasma current I_p^{max}, safety factor q_a, mean current density $\bar{j}=I_p^{max}/\pi ab$ and elongation ratio κ on this measured value n_0 under the active control of the shaping field. The safety factor q_a was estimated under the assumption of a flat current profile and an elliptical cross section ($q_a=2\pi a^2 B_t/\mu_0 R_0 I_p \cdot (1+\kappa^2)/2$). With the decrease in n_0 down to $\simeq -0.6$, I_p^{max}, κ and the discharge duration increase, while V_l

decreases. In the case of $n_0 \simeq -0.6$, the optimum parameters are $\kappa \simeq 1.5$, $q_a \simeq 2.4$ and $I_p^{\max} = 24$ kA. When n_0 changes from -0.2 to -0.8, $\bar{j}$ gradually goes up by about 10%. From this figure, it is given that $I_p^{\max}$ increases with κ. Due to the peaking of the current density profile, elongation ratio drops in the case of $n_0 \simeq -0.75$. (Elongation ratio is smaller with peaked current density profile when n is fixed.[15,16]) From the equilibrium code EQUCIR,[17] elongation ratio κ increases with the flatter current profile (internal inductance l_i is lower) and the increase in triangularity γ when the decay index n is fixed. With the same values of γ and l_i, κ decreases with n. In the lowest graph in Fig. 6, these numerical curves are also shown. The fitting parameters with the measurements are $\gamma \sim 0.5$ when $l_i \sim 0.55$ (nearly flat current profile) and $\gamma \sim 0.6$ when $l_i \sim 0.92$ (parabolic current profile).

The maximum plasma current was limited at a level of $q_a > 2$. (The low frequency MHD oscillation ($f \leq 40$ kHz) of $m=2$ mode is high level near the current peak.) Up to now, a stable plasma has been obtained when $n_0 \gtrsim -0.9$ was satisfied. A rough estimate[18] of the stabilization on the positional instability was done, assuming the rigid shift of the plasma column. This calculation shows that this instability is suppressed by the shell.

The active and passive control was employed, i.e., two sets of the top and bottom shaping coils were connected in series to act as a shell on the vertical motion of the plasma. The discharge duration became longer by $1 \sim 2$ ms and the activity of the loop voltage at the current decreasing stage was quieter and the rate of the vertical shift was smaller than in the case of the active control only, although the passive coils were relatively far away from the plasma surface.

§6. Conclusion

The effect of the decay index on the plasma shaping has been investigated over a wide range ($-0.9 < n_0 < -0.2$) in TNT-A machine. It was shown that $I_p^{\max}$, κ and j increased with the decrease in n_0 until $n_0 \simeq -0.6$, while $q_a > 2$ (low frequency oscillation of $m=2$ mode appears) was satisfied. In the case of $n_0 \simeq -0.6$, a D-shaped plasma of $I_p^{\max} = 24$ kA, $q_a \simeq 2.4$, $\kappa \simeq 1.5$, $T_{e0} \sim 180$ eV, $n_{e0} \sim 10^{13}$ cm^{-3} was obtained. That is, we have successfully produced the stable plasma with elongation of up to 1.5 and relatively low safety factor ~ 2.4. Plasma shape by measurements fitted well with the calculation in the case of $l_i \sim 0.5$–0.9 and $\gamma \sim 0.5$–0.6.

The lower limit of the decay index to obtain the stable plasma was $n_0 \gtrsim -0.9$, which is supposed to be determined by the stabilizing force of the shell. Although the passive shaping coils were relatively far from the plasma, the active and passive control made the discharge duration longer by $1 \sim 2$ ms, the activity of the loop voltage quieter and the rate of the vertical shift smaller than the active control only did.

The effects of the iron core and shell on the decay index plays an important role in a non-circular cross section plasma. From the term of the shaping current, the iron core makes the decay index lower, and the shell makes the field curvature smaller, especially near the surface of the iron core and shell. The calculation and the measurements showed that the decay index is affected mainly by the iron core.

The results of the relation between the decay index and elongation ratio will be the basis of making the desired elongated plasmas by the applied external field in a large machine. The measurements and the calculation of the decay index in the presence of the iron core and shell are also useful to design a large device.

Acknowledgements

The authors are grateful for helpful discussions and information with Professor S. Yoshikawa, Professor K. Miyamoto and Mr. H. Kaneko, and thank Mr. S. Tsuji for his valuable assistance in performing the experiments.

References

1) T. Ohkawa: Kaku Yugo Kenkyu **20** (1968) 557.
2) D. Dobrott and M. S. Chu: Phys. Fluids **16** (1973) 1371.
3) L. A. Artsimovich and V. D. Shafranov: Pis'ma Zh. Exsp. & Teor. Fiz. **15** (1972) 72. translation: Sov.Phys.- JETP Lett. **15**(1972) 51.
4) R. L. Freeman *et al.*: in *Plasma Physics and Controlled Nuclear Fusion Research (Proc. 6th Conf., Berchtesgaden, 1976)* **1**, IAEA, Vienna (1977) 317.

5) A. J. Wootton and D. C. Robinson: in *Proceedings of 8th European Conference on Controlled Fusion and Plasma Physics, Prague*, **1** (1977) 42.
6) K. McGuire, D. C. Robinson, A. J. Wootton: in *Plasma Physics and Controlled Nuclear Fusion Research (Proc. 7th Conf. Innsbruck, 1978)* **1**, IAEA, Vienna, (1979) 335.
7) J. J. Ellis, K. McGuire, P. Peacock, D. C. Robinson, I. Stares: in *Plasma Physics and Controlled Nuclear Fusion Research (Proc. 8th Conf., Brussels, 1980)* **1**, IAEA, Vienna (1981) 731.
8) JAERI Team: Nucl. Fusion **20** 11 (1981) 1455.
9) M. Nagami *et al.*: Nucl. Fusion **22** 2 (1982) 3.
10) INTOR Group: Nucl. Fusion **20** 3 (1980) 353.
11) H. Toyama *et al.*: in *Plasma Physics and Controlled Nuclear Fusion Research (Proc. 6th Conf., Berchtesgaden, 1976)* **1**, IAEA, Vienna (1977) 323.
12) H. Toyama *et al.*: in *Plasma Physics and Controlled Nuclear Fusion Research (Proc. 7th Conf., Innsbruck, 1978)* **1**, IAEA, Vienna (1979) 365.
13) K. Toi *et al.*: in *Plasma Physics and Controlled Nuclear Fusion Research (Proc. 8th Conf., Brussels, 1980)* **1**, IAEA, Vienna (1981) 721.
14) P. W. Swain, S. Bates, G. H. Neilson, Y-K. M. Peng: ORNL/TM-7172 (1980).
15) A. Iwahashi, I. Ochiai, H. Toyama: J. Phys. Soc. Jpn. **45** (1978) 289.
16) S. Shinohara, K. Sakuma, S. Tsuji, and H. Toyama: J. Phys. Soc. Jpn. **48** (1980) 1051.
17) H. Ninomiya, K. Shinya and A. Kameari: *Proc. 8th Sympo. on Engineering Problems of Fusion Research*, **1** (1979) 75.
18) S. Shinohara and H. Toyama: J. Phys. Soc. Jpn. **49** (1980) 1965.